Plant Science 338 (2024) 111900

Contents lists available at ScienceDirect

Plant Science

journal homepage: www.elsevier.com/locate/plantsci

PLAT domain protein 1 (PLAT1/PLAFP) binds to the *Arabidopsis thaliana* plasma membrane and inserts a lipid

Martin Kulke [a,1], Evan Kurtz [b,2], Duncan M. Boren [a,b], Dayna M. Olson [b], Amanda M. Koenig [b,3], Susanne Hoffmann-Benning [b,*], Josh V. Vermaas [a,b,**]

[a] Plant Research Laboratory, Michigan State University, East Lansing 48824, MI, USA
[b] Department Of Biochemistry and Molecular Biology, Michigan State University, East Lansing 48824, MI, USA

ARTICLE INFO

Keywords:
Molecular Dynamics Simulations
Protein-Membrane Interactions
Phosphatidic Acid
Protein-Lipid Interactions
Lipid Transport
Lipid Insertion

ABSTRACT

Robust agricultural yields depend on the plant's ability to fix carbon amid variable environmental conditions. Over seasonal and diurnal cycles, the plant must constantly adjust its metabolism according to available resources or external stressors. The metabolic changes that a plant undergoes in response to stress are well understood, but the long-distance signaling mechanisms that facilitate communication throughout the plant are less studied. The phloem is considered the predominant conduit for the bidirectional transport of these signals in the form of metabolites, nucleic acids, proteins, and lipids. Lipid trafficking through the phloem in particular attracted our attention due to its reliance on soluble lipid-binding proteins (LBP) that generate and solubilize otherwise membrane-associated lipids. The Phloem Lipid-Associated Family Protein (PLAFP) from *Arabidopsis thaliana* is generated in response to abiotic stress as is its lipid-ligand phosphatidic acid (PA). PLAFP is proposed to transport PA through the phloem in response to drought stress. To understand the interactions between PLAFP and PA, nearly 100 independent systems comprised of the protein and one PA, or a plasma membrane containing varying amounts of PA, were simulated using atomistic classical molecular dynamics methods. In these simulations, PLAFP is found to bind to plant plasma membrane models independent of the PA concentration. When bound to the membrane, PLAFP adopts a binding pose where W41 and R82 penetrate the membrane surface and anchor PLAFP. This triggers a separation of the two loop regions containing W41 and R82. Subsequent simulations indicate that PA insert into the β-sandwich of PLAFP, driven by interactions with multiple amino acids besides the W41 and R82 identified during the insertion process. Fine-tuning the protein-membrane and protein-PA interface by mutating a selection of these amino acids may facilitate engineering plant signaling processes by modulating the binding response.

1. Introduction

Based on current crop yield projections coupled to population growth, food scarcity is projected to increase through 2050, Ray et al. (2013) with uncertainty in the modeling around plant temperature responses playing a major role Wang et al. (2017). Strategies to improve crop production include approaches that enhance plant resilience to abiotic stressors such as drought, salinity, flooding and extreme temperatures Bailey-Serres et al. (2019). Understanding the underlying molecular mechanism is important to design improved response pathways (Lin et al., 2019; Mega et al., 2019; Munns et al., 2012; Liu et al., 2021). The current concept involves a cascade of processes, including sensing, signaling, transcription, translation and post-translational protein modifications to improve crop robustness to a varying climate Zhang et al. (2022).

Environmental changes trigger both intracellular local signaling and long-distance/systemic signaling. It is essential to understand the signaling processes that coordinate responses between local tissues,

* Corresponding author.
** Corresponding author at: Plant Research Laboratory, Michigan State University, East Lansing 48824, MI, USA.
E-mail addresses: hoffma16@msu.edu (S. Hoffmann-Benning), vermaasj@msu.edu (J.V. Vermaas).
[1] Current address: TUM School of Natural Sciences, Technische Universität München, Munich, Germany.
[2] Current address: Department of Biochemistry and Biophysics, Texas A&M University, College Station, TX 77843, United States of America.
[3] Current address: Plant Research Laboratory, Michigan State University, East Lansing, MI 48824, USA

https://doi.org/10.1016/j.plantsci.2023.111900
Received 16 May 2023; Received in revised form 14 September 2023; Accepted 16 October 2023
Available online 19 October 2023

which are perceiving the stress, and the distal tissue throughout the whole plant (Lucas et al., 2013; Notaguchi and Okamoto, 2015). Lacking a nervous system, plants have developed sophisticated translocation networks through the phloem, which transport various mobile molecules, such as metabolites, secondary messengers, small proteins, and RNAs, to connect and share information between tissues Takahashi and Shinozaki (2019). In recent years, phospholipids have been proposed as long distance signals, but their importance in plants is largely unexplored (Guelette et al., 2012; Benning et al., 2012; Barbaglia and Hoffmann-Benning, 2016; Koenig et al., 2020). In the past, PA has been shown to be a major intracellular signal in response to a variety of abiotic and biotic stresses (Munnik, 2001; Wang, 2004; Testerink and Munnik, 2005; Wang et al., 2007; Testerink and Munnik, 2011; Wang and Chapman, 2013; Kim and Wang, 2020; Ali et al., 2022). Furthermore, the presence of PA in phloem exudates suggests a function for PA in long-distance signaling as well Guelette et al. (2012). The hydrophobic nature of the lipids requires transport proteins to sequester the acyl chains away from the aqueous environment in the phloem.

One candidate for lipid transport or as co-signal is the Phloem Lipid-Associated Family Protein (PLAFP) that is hypothesized to transport PA through the phloem in response to drought stress Benning et al. (2012). PLAFP contains a PLAT/LH2 domain, formed by a β-sandwich of two β-sheets with four β-strands each, and a C-terminal α-helix. *PLAFP* is expressed in leaf and root vasculature in three week-old seedlings and in mature plants (Barbaglia et al., 2016; Hyun et al., 2014), and more specifically has been shown to be expressed in companion cells Mustroph et al. (2009). The abundance of PA McLoughlin and Testerink (2013) and the expression of *PLAFP* (Barbaglia et al., 2016; Hyun et al., 2014) are both upregulated in the presence of abscisic acid (ABA), a drought stress signaling compound Ali et al. (2020). *PLAFP* expression is also upregulated in the presence of the water-stress mimicking molecule polyethylene glycol Barbaglia et al. (2016).

Cellular localization studies show that PLAFP is localized in a spotted pattern around the periphery of the cell and not retained in the endoplasmic reticulum (ER) Barbaglia et al. (2016). Additionally, PLAFP binds specifically to PA in lipid overlay and liposome-binding assays (Benning et al., 2012; Barbaglia et al., 2016). Together, these findings suggest that PLAFP and PA are both produced during drought stress and localize at the plant plasma membrane, where PLAFP desorbs PA from the membrane and transports the lipid through the phloem for signaling (Fig. 1) (Barbaglia and Hoffmann-Benning, 2016; Koenig et al., 2020). Target receptor proteins for the PLAFP-PA complex are currently unresolved.

In this study, we leverage the spatial and temporal resolution of molecular simulation to quantify the nanoscale mechanism behind hypothesized PLAFP function by tracking PLAFP binding to a plant plasma membrane model, and subsequent insertion of anionic PA lipids into the β-sandwich of PLAFP. We find that PLAFP binds to plasma membranes independent of the membrane PA content in a consistent stable binding pose by anchoring W41 and R82 into the hydrophobic core of the membrane. After membrane association, PLAFP undergoes a conformational change, where the separation distance between W41 and R82 increases, which we hypothesize triggers PA-binding. PA inserts with the lipid tails into a hydrophobic pocket in PLAFP between the two β-sheets, while the charged lipid head group remains exposed for potential receptor interactions. The insertion of PA weakens the PLAFP-membrane interactions leading to the dissociation of the PLAFP-PA complex from the plasma membrane, which would then be transported by the phloem stream.

2. Methods

2.1. PLAFP subcellular localization using confocal microscopy

CaMV35S::PLAFP-eYFP (pPZP212) Barbaglia et al. (2016) was transformed into *Agrobacterium tumefaciens* GV3101 by electroporation and selected with 50 μg/mL kanamycin, 10 μg/mL gentamicin, and 10 μg/mL rifampicin. The plasma membrane marker (PM-RK) Nelson et al. (2007) and PLAFP-eYFP in A. tumefaciens GV3101 were grown in 25 mL cultures in Luria Broth (100 μM acetosyringone, 50 μg/mL kanamycin, 10 μg/mL gentamicin, and 10 μg/mL rifampicin) at 28°C to an OD600 of 0.6. The cells were harvested by centrifugation at 3000 xg for 10 min. The cell pellets were resuspended in infiltration buffer (10 mM MES pH 5.7, 10 mM MgCl, 100 μM acetosyringone) to an OD600 of 0.6. Resuspended cells were incubated at room temperature for 1–3 h then individually infiltrated into *Nicotiana tabacum* with a 1 mL needleless syringe. The resuspended PLAFP-eYFP and PM-RK cells were combined 1:1 by volume, briefly vortexed, and co-infiltrated into another N. tabacum leaf. Infiltrated tobacco was left in the Percival growth chamber at 22°C on a 12–12 day/night cycle for 2 days. The spectral-based Olympus FluoView 1000 confocal laser-scanning microscope was used to image eYFP (PLAFP) and mCherry (PM-RK) in infiltrated tobacco leaves. The eYFP and mCherry fluorescence was excited with the 515 nm and 559 nm lasers, respectively. The eYFP emission was captured between 530 and 560 nm and mCherry between 570 and 600 nm.

2.2. Protein model

No experimentally determined structure exists for PLAFP. Thus,

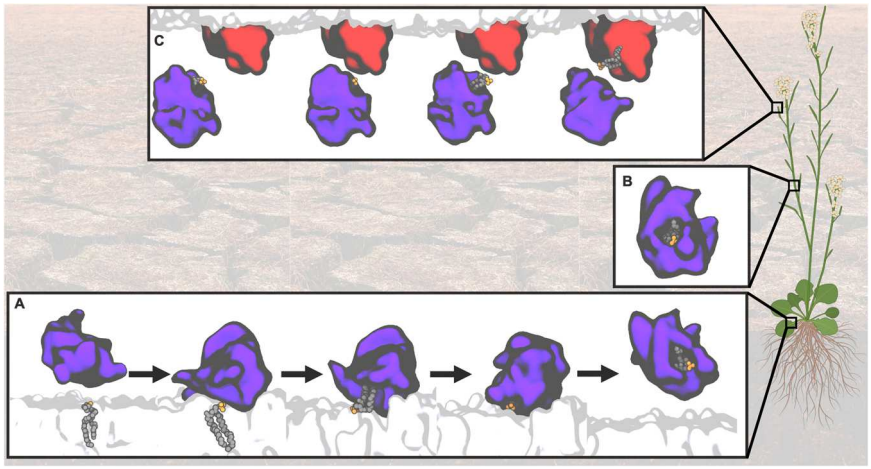

Fig. 1. Schematic showing a proposed model for PLAFP-PA systemic signaling: **A** PLAFP (purple) extracts PA from the plasma membrane and inserts the lipid into a hydrophobic pocket. **B** Afterwards, the protein-lipid complex travels through the phloem and **C** binds to an unknown receptor protein (red) in a distal tissue.

homology modeling to determine the 3D protein structure is required prior to simulation. PLAFP has a signal peptide that is cleaved off after import into the ER. The mature sequence (uniprot id: O65660) The UniProt Consortium (2015) used for modeling spans residues 24–181, which has a 24.6% sequence identity with the nearest structurally resolved sequence of calcium-dependent 11R-lipoxygenase (pdb code: 3VF1) Renatus et al. (1997). Multiple homology models were constructed using the Robetta (Källberg et al., 2012; Söding, 2005; Yang et al., 2011; Ovchinnikov et al., 2017; Yang et al., 2020; Baek et al., 2021; Song et al., 2013), Swiss (Bienert et al., 2017; Studer et al., 2020; Bertoni et al., 2017; Waterhouse et al., 2018) and iTasser (Yang et al., 2014; Roy et al., 2010; Zhang, 2008) modeling server (Fig. 2A,B). To evaluate the structural stability for the homology models, each model was solvated in explicit water including 0.15 mol L^{-1} NaCl and simulated at 298 K and 1 bar for 100 ns following a short 100 ps equilibration period. We selected one of the Robetta predictions as final model based on: (i) structural stability during the molecular dynamics simulation, (ii) a high content of structural elements and (iii) a high sequence identity and homology modeling scoring factor (Fig. S2). Details to the selection process are described in the Supporting Information.

2.3. Membrane-PLAFP interaction simulations

The membrane composition is obtained from *Arabidopsis thaliana* plasma membrane lipidomics data from existing literature (Grison et al., 2015; Uemura et al., 1995). Three different membranes with varying PA content and 46% sterols, 7% ceramides, 47% phospholipids, and an explicit water interphase were generated in a $10.2 \times 10.2 \times 8.5$ nm^3 rectangular box using the membrane builder interface within CHARMM-GUI (Lee et al., 2016; Wu et al., 2014; Jo et al., 2008). Membrane 1 lacks PA, membrane 2 has near-native PA content, and membrane 3 is enriched with 3x the typical PA content (Table S1).

To assess binding in an unbiased manner, the PLAFP protein center of mass was placed 4.7 nm above each of the three membranes along the z-axis, the membrane surface normal, for six different orientations, each orientation representing the face of a cube (Fig. 2B). Four of these orientations were rotations around the x-axis at 0°, 90°, 180°, and 270° and the other two were rotations around the y-axis at 90° and − 90°. In this position, the protein was above the water interface generated by CHARMM-GUI with a few orientations slightly touching into the water phase. The z-axis of the simulation box was adjusted to approximately 14 nm to fit the additional space generated by the protein. After solvating this space with the `solvate` command in VMD 1.9.4a55 Humphrey et al. (1996), the membrane occupied ~ 4 nm and the water phase ~ 10 nm in the z-axis. The sodium chloride concentration was set to 0.15 mol L^{-1} neutralizing the system by replacing water atoms with ions. Because lateral lipid diffusion within the membrane is slow compared to the simulation timescale and the membrane has 22 unique components, simulations are biased by the initial lipid and sterol starting positions. Therefore, sampling statistics were improved by replicating each orientation five times with independently generated sterol and lipid starting positions within the membranes, resulting in 90 total simulations (3 membranes, 6 orientations, and 5 replicas). All systems were simulated for 200 ns.

2.4. PA-PLAFP insertion simulations

The conformation with PLAFP in the most probable membrane binding state, where W41 and R82 are separated and anchored in the membrane, was taken from the membrane-PLAFP interaction simulations. In a new simulation system, this conformation was then solvated with explicit water and neutralized with 0.15 mol L^{-1} NaCl in a $10 \times 10 \times 10$ nm^3 box and one PA lipid was placed in the proximity of the R82 residue (Fig. 2C). Flat-bottom constraints between the lipid head group phosphorus atom and five heavy atoms in the surrounding location restricted the lipid conformation sampling space to below 15 Å

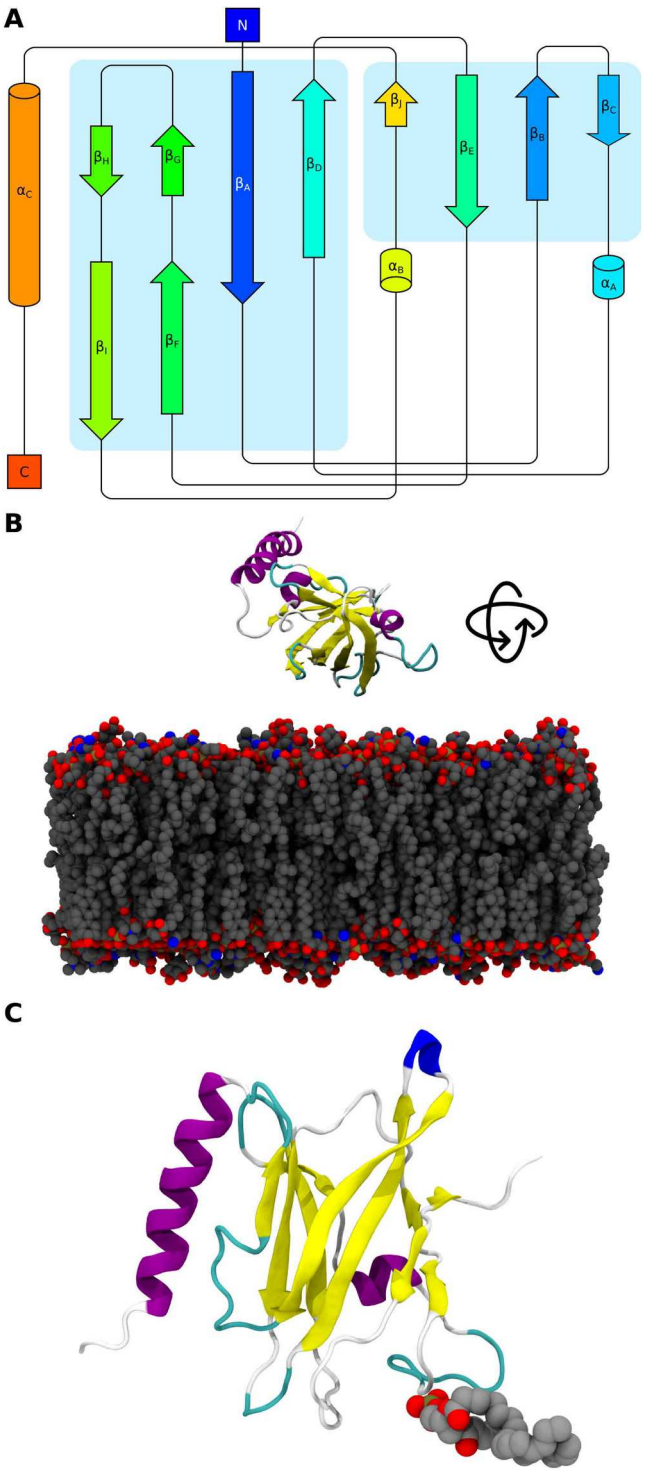

Fig. 2. **A** The secondary structure elements of PLAFP. The colorscale follows the protein backbone from the blue N- to red C-terminus. Arrows on a teal background indicate antiparallel β-sheets. Cylinders represent α-helices. **B** Starting state of the PLAFP-membrane interaction simulations with the protein floating right above the plasma membrane. Replica systems with six different protein rotations around the x- and y-axis were simulated. Membranes were modeled according to published plasma membrane compositions (Grison et al., 2015; Uemura et al., 1995) (see Table S1). **C** PLAFP in cartoon representation with one PA lipid in the proximity of the binding pocket shown as van-der-Waals balls.

around the R82 and W41 region with a force constant of 100 kcal/mol/Å^2. The system was replicated 9 times and simulated for 1.8 μs each.

2.5. Membrane PA-PLAFP interaction simulations

PLAFP with inserted PA was taken from the final frame of the PA-PLAFP insertion simulations first replica. The complex was placed above the plasma membrane in different orientations with the preparation procedure described in the Membrane-PLAFP interaction simulations section. The resulting 30 total simulations (6 orientations with 5 replica each) were simulated for 200 ns.

2.6. Molecular dynamics simulations

NAMD 3.0a9 Phillips et al. (2020) was used as the molecular dynamics engine to simulate the systems enumerated above using the CHARMM36m force field for proteins Huang et al. (2016), lipids Klauda et al. (2010), and ions Beglov and Roux (1994). Water was represented with the TIP3P water model Jorgensen et al. (1983). The equation of motion is evaluated by a verlet integrator every 2 fs applying periodic boundary conditions to the simulation system. Short-range electrostatic and van der Waals interactions are calculated for atom pairs within 12 Å with a switching function beginning at 10 Å shifting the force to zero at the cutoff using the vdwForceSwitching argument. Long range electrostatics are calculated with PME in a 1.2 Å spaced grid Essmann et al. (1995). Atom pairs are tracked in interaction pair lists generated every 200 fs for pairs within 14 Å distance. Temperature is controlled by a Langevin thermostat to 300 K with damping coefficients of 1 ps^{-1} for all atoms Grest and Kremer (1986). Pressure is adjusted to 1 atm by a Nosé -Hoover Langevin piston with a 200 fs oscillation period and a 100 fs damping time scale Feller et al. (1995). In membrane systems, the different compressibilities for the membrane and water phase are accounted for by semiisotropically adjusting the pressure along the membrane surface plane and normal vector. Bonds in water molecules are constrained with SETTLE Miyamoto and Kollman (1992), while all other bonds that include a hydrogen atom are constrained with the SHAKE algorithm Ruymgaart and Elber (2012).

2.7. Contact number and penetration depth

Each trajectory was analyzed in VMD 1.9.4a55 Humphrey et al. (1996) visually, and its scripting capabilities were used to quantify contacts between protein and membrane, and membrane penetration depths. The data was further analyzed with python 3.8.5 Van Rossum and Drake (2009) utilizing the numpy Harris et al. (2020) and matplotlib Hunter (2007) libraries for analysis and data visualization.

Contact numbers are determined by the heavy atoms of a protein residue and a membrane lipid coming within 6 Å distance. To account for differences in contact strengths C, a contact is scaled according to its distance d using a sigmodial function derived from protein folding studies (Sheinerman and Brooks, 1998), and previously used to quantify membrane-protein contact (Vermaas and Tajkhorshid, 2017):

$$C = \frac{1}{1 + e^{5\times(d-4\text{Å})}} \quad (1)$$

Average contact numbers are time averaged over the trajectory frames. Since the starting position of the protein is near the membrane, the initial diffusion period where the protein drifts to the membrane is short. Nevertheless, the first 75 ns of each trajectory were omitted from the analysis to promote an unbiased equilibrated structural ensemble of the protein-membrane interactions (Fig. S3).

Membrane penetration depths of individual protein residues were quantified by calculating the probability densities of the minimum z-distance in relation to the membrane center for individual amino acids and lipid phosphorus atoms. Since the composition of the membrane upper and lower leaflet are identical in our membrane construction, the absolute values for the z-distances are considered to increase the sampling.

3. Results

3.1. PLAFP interacts with the plant plasma membrane

Confocal microscopy shows that PLAFP is associated with the plant plasma membrane, with PLAFP co-localized with plasma membrane markers (Fig. 3), consistent with prior localization to the cell periphery Barbaglia et al. (2016). The spotted pattern for localization in Fig. 3 suggests association near the plasmodesmata, based on similar patterns observed in other plasmodesmata-associated proteins Ishikawa et al. (2017). However, the mechanism and orientation of the interaction remains unknown. To further investigate the binding orientation and geometry of PLAFP with the plasma membrane, the interactions between PLAFP and the plasma membrane were simulated in 90 simulations. Interactions were quantified by counting contacts between protein and lipids over the trajectory frames, as well as monitoring insertion depth. Each of the simulations was 200 ns long and independent, varying the initial lipid starting positions, PA concentrations in the membrane based on experimental lipidomics studies (Grison et al., 2015; Uemura et al., 1995), and initial protein orientations with respect to the membrane surface, as indicated in the methods. The average area per lipid and average order parameter of the membranes equilibrated within the first 50 ns of each simulation (Figs. S4 and S5) to the liquid ordered phase (Fig. S6), because of the high sterol content, which reduced lateral lipid diffusion tenfold compared to liquid disordered membranes Kulke et al. (2023) (Fig. S7).

We find that PLAFP interacts with the plasma membrane in most of the replicate simulations, and does so for the overwhelming majority of the simulation time (Fig. S3). In 17% of trajectories, the binding interaction was not durable, and PLAFP moved into solution during the simulation overall resulting in 28–31% unbound frames for each membrane composition. However, in all frames with bound PLAFP, the protein was observed to bind primarily in one single overall orientation (Fig. 4), with a consistent set of residues coming into close proximity to the membrane (Figs. 5, S8). In this orientation, PLAFP presents the two flexible loops βL_A and βL_C towards the membrane (Movie S1). Upon binding, these loops are inserted inside the membrane with a penetration depth of 0.3–0.5 nm with respect to the membrane phosphate plane (Fig. 6). The amino acids with the greatest membrane penetration are W41 and R82, each at the tip of the respective flexible loops. W41 in particular is observed to strongly interact with the hydrophobic membrane core potentially driving membrane penetration for adjacent residues. After the penetration event occurred, PLAFP did not unbind from the plasma membrane within the simulation time. Other residues with significant lipid interactions are R36, S39, I40, K42, N84, and the amino acids at the end of C-terminal α-helix (Fig. 5). Membrane interactions are also observed for the surface of the β-sheet, as the protein sporadically lays flat onto the membrane surface with the β-sheet surface in contact.

Unlike for binding to PC or PIPs, there are no conserved binding-domains known for interaction with PA. Instead the general requirement appears to be a series of basic amino acid side chains in the proximity of a hydrophobic pocket. Basic residues such as R36, K42 and R82 are conserved among multiple PLAFP homologues and are predicted to interact with PA (Awai et al., 2006; Testerink et al., 2007; Wang et al., 2013; Li et al., 2013; Rice and Wereszczynski, 2017). During the simulation, the membrane interacts preferably with R82, suggesting that the R82 loop engages in more durable interactions with the membrane compared to the loop containing W41. Given the short sequence distance between W41, R36, and K42, we propose that W41 sterically hinders other neighboring amino acids in its loop to deeply penetrate the membrane and interact strongly with phosphate headgroups relative to

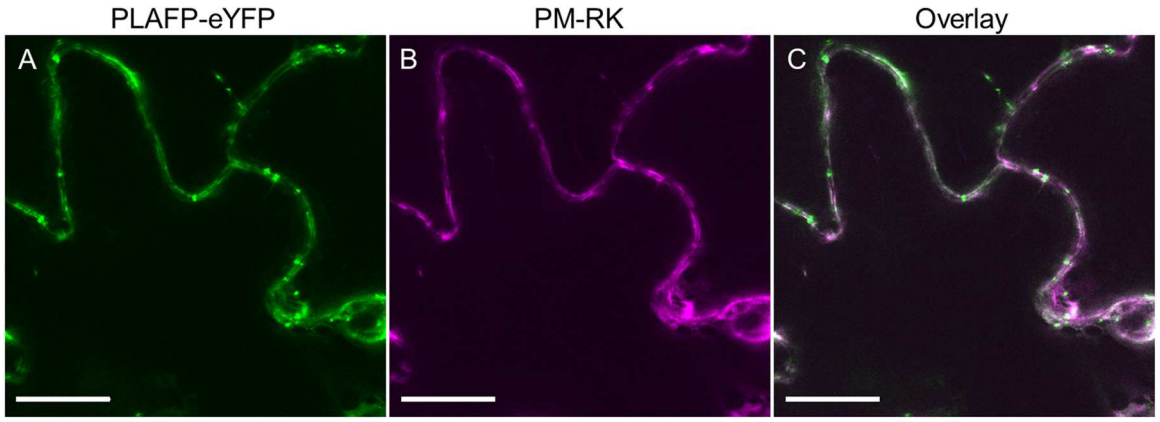

Fig. 3. Confocal microscopy images of PLAFP localizing with the plasma membrane. **A** PLAFP-eYFP in green is observed in the periphery of tobacco epidermal cells and exhibits a punctuate pattern, which may indicate association to the plasmodesmata or another specific structure at the membrane surface. PLAFP co-localizes with **B** the plasma membrane marker PM-RK Nelson et al. (2007) in magenta, as observed in white in the overlay **C**, which indicates overlap between the PLAFP and plasma membrane marker signals. Scale bar represents 20 μm.

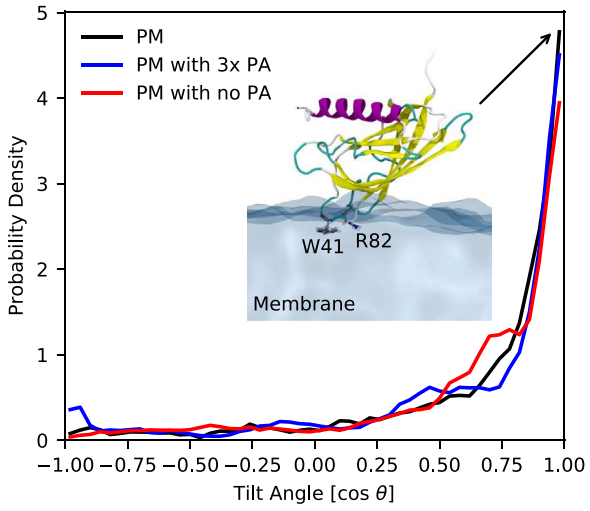

Fig. 4. Conformational probability density of the tilt angle deviation relative to the structure shown as inset, which is PLAFP's preferred binding pose. In this conformation PLAFP in cartoon representation anchors to the plasma membrane shown as transparent lightblue surface. Tilt angles are measured with respect to the membrane surface normal vector, and tilt angles of $cos\theta = 1$ correspond to the structure shown in the inset, while protein conformations perpendicular and anti-parallel to this structure have values around 0 and − 1, respectively. Probability densities are calculated from the united replicate trajectories for each membrane composition.

R82. Rather than lead to membrane association, R36 or K42 may have other roles within the membrane-protein association process.

Although PLAFP was shown to interact with PA *in vitro* in previous studies (Benning et al., 2012; Barbaglia et al., 2016), this interaction is not required for the protein to associate to the plasma membrane. PLAFP bound in similar orientations irrespective of the PA concentration in the membrane, with similar insertion depths (Fig. 6). Quantifying contacts per residue again show highly similar trends, regardless of the PA concentration present in the membrane (Fig. 5). Independent of the plasma membrane having no PA, the natural amount, or three times the natural amount, PLAFP did interact with the plasma membrane in the same conformation (Fig. 6) and with equal strength (Fig. 5). Phospholipids make up the overwhelming majority of interactions to the protein with PC and PE having the highest interaction, but they are also the most abundant phospholipids (Table S2). Charged lipid head groups PI, PS and PA do not have significantly more interactions than what is expected based on their molecule count. Thus, within the limits of our molecular sampling, different phospholipids contribute equally to the total interaction count, suggesting that membrane association is non-specific to the lipid headgroup. However, since so many protein-membrane interactions are to the phospholipid headgroups, sterols are underrepresented in the interaction with PLAFP. Sterols make up 46% of the plasma membrane composition, but since they are largely hydrophobic with only minimal hydroxyl headgroups, they do not make as many contacts as the surrounding phospholipids do.

3.2. PA inserts into PLAFP

When visually analyzing the membrane-protein interaction trajectories, we observed that the protein conformation is not static, but instead undergoes a membrane-induced conformational change in the two loop regions L_A and L_C that are in direct contact with the membrane surface. While in solution, these loops demonstrate a tight distribution of distances, indicating specific interactions or solvent effects that drive the loops together (Fig. 7A,B). As the loops come into proximity with the membrane, alternative interaction partners are available to the loops, and the loops are observed to separate up to a distance of 2 nm, opening a cavity within the protein (Fig. 7A,C).

Our initial hypothesis was that this cavity acts as an acceptor for lipid acyl tails, lowering the barrier for desorbing PA acyl tails from the membrane core. To test this hypothesis, a protein-lipid system with PLAFP and one PA lipid placed near this binding cavity in aqueous solution were simulated in nine replicas (Movie S2). The initial binding of PA to PLAFP occurs in four states, whereby two of the states lead to further insertion of PA into PLAFP, and two are traps that hinder insertion for up to a few microseconds. Out of the nine replicas, in six PA did bind initially into trap states a or b, in two replicas into state c and in one replica into state e (Fig. 8). Trap state a is characterized by the PA head group being immobilized between L_A and L_C interacting with R82, R36 and T37. Sporadically, the head group will interact with K42 instead of R82. The lipid tails are directed toward the β-sheets β_I and β_F interacting with I40, Y116, W141, and W41. The head group interacting with R82 and the tails with W41 results in a stable separation of these two amino acids. In trap state b, the lipid head group interacts with R82 or K42 from the opposite site, while the tails in this state wrap around L_A towards L_E and L_I interacting with H112, W141, T146, A143, I40 and D145 (Fig. 8). The separation of W41 and R82 is not required in state b.

We did observe the transition between the two trap states a and b, but in the simulations only trap state b did transition into state e to initiate the insertion process. This happens by the lipid tails flipping around to the opposite site into the space between L_A and L_C towards α_A.

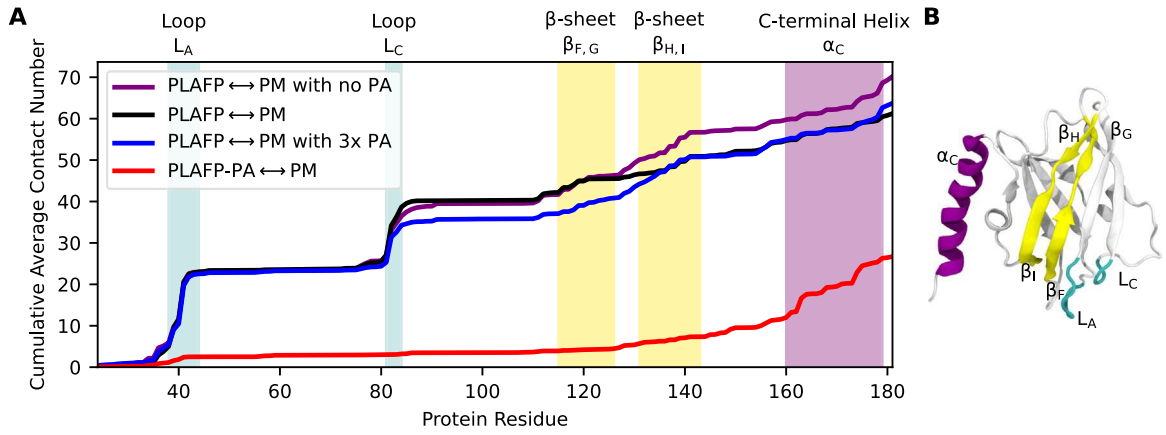

Fig. 5. **A** Average contact number per protein residue to phospholipids, reported as a cumulative sum. Protein elements with many binding interactions will cause the line to rise at that point. Regions of interest are colored after their secondary structure element, which are **B** visualized onto the tertiary structure of the protein. In **A**, the purple, black, and blue traces track PLAFP without a bound lipid interactions with the membrane, while the red trace tracks the contacts with the membrane once a PA lipid is bound to PLAFP.

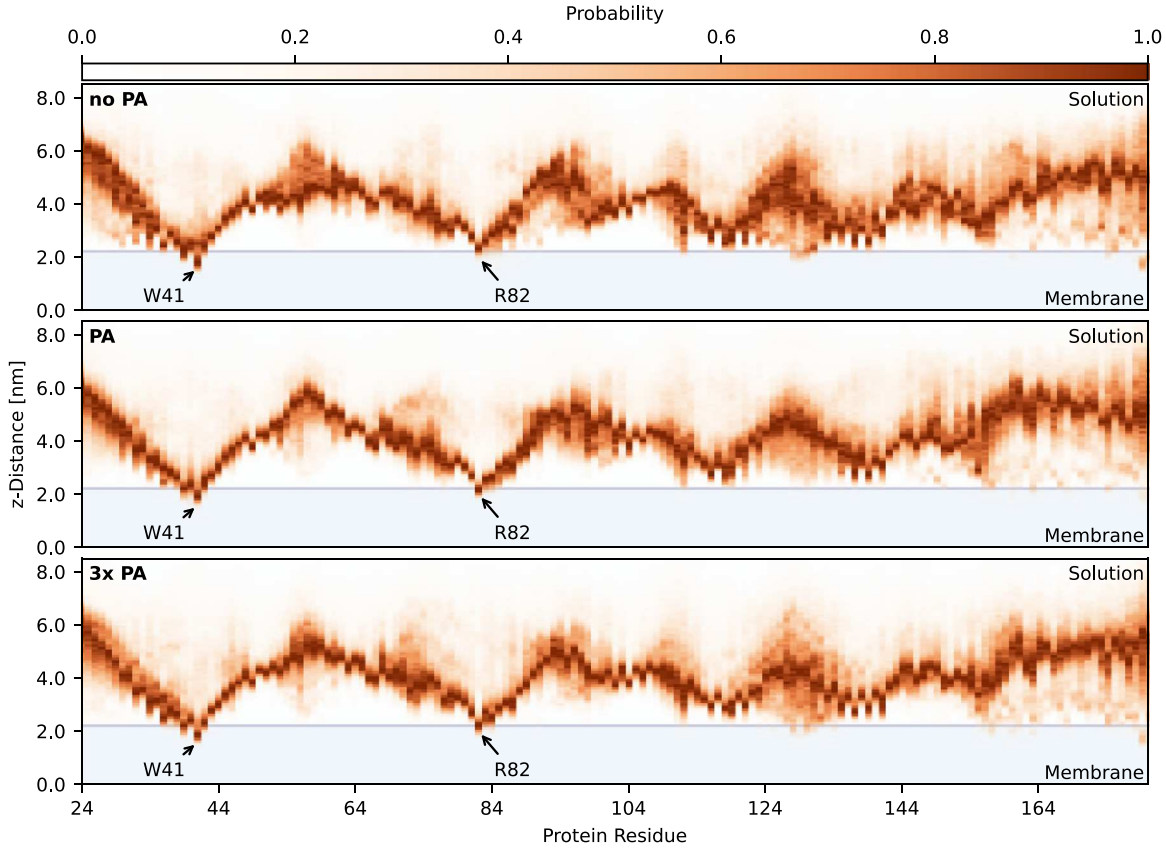

Fig. 6. Probability density profiles of the minimum distance between each protein residue and the membrane center. The membrane phase is shown as blue-shaded area and the aqueous phase in white. The probability to find a residue at a certain distance away from the membrane center is colored in shades of red. Red colors that overlap with blue regions indicate residues that penetrate the membrane surface.

During the process, the lipid head group keeps interacting with R82, and is further stabilized by T45 and D46 at the end of the flip. The tails start to interact with I48, N65, Q67, A68, Y77, Y79, and F80. Subsequently, either the lipid head group partially inserts into the pocket between L_A and L_C driven by interactions with W115, R82, and D86 (Fig. 8f), or one of the lipid tails slips into the same pocket. Either way, interactions between the lipid tail ester group and W115 drives the deep insertion of the first lipid tail, while simultaneously separating W41 and R82. During the insertion process, the lipid phosphate group is slightly pushed out of the pocket, and interacts solely with R82 while the remainder of the lipid moves further towards α_A (Fig. 8g). In some simulations, the lipid head group was positioned between W41 and R82 to make more space inside the binding pocket and allowing the lipid tail to insert correctly. In state g, the lipid tail is located inside the hydrophobic protein core in between the β-sandwich interacting with multiple hydrophobic amino acids Y31, F33, I53, I59, I63, L66, W69, F88, L95, L104, W115, V120, and I122. Between the β-sandwich is enough space for both lipid tails, and the insertion of the second tail did take up to several 100 ns in the

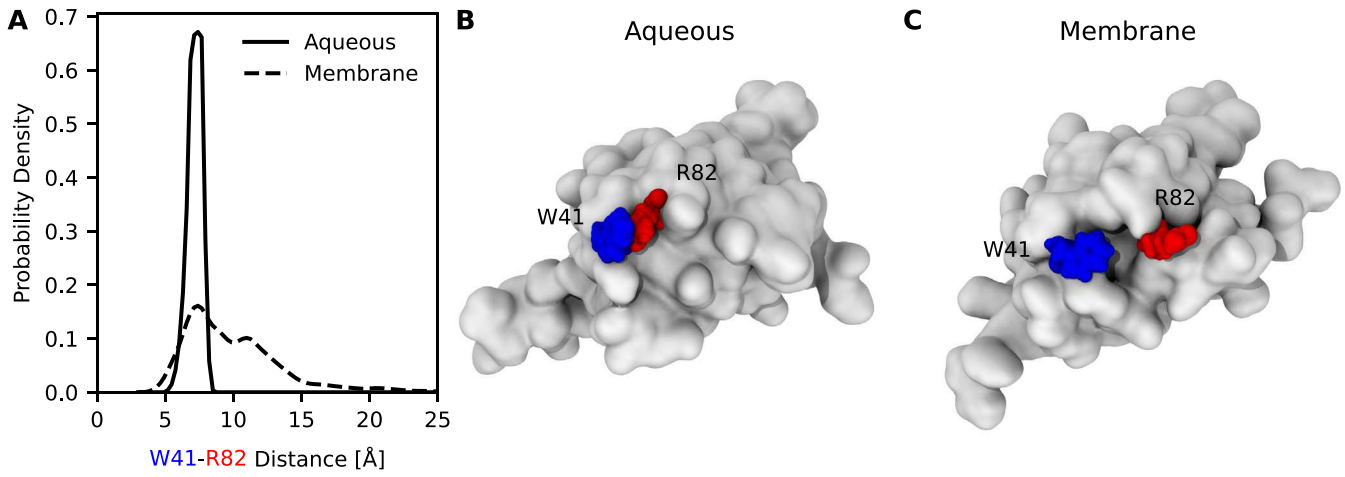

Fig. 7. **A** Histograms of the distance between the C_α atoms of R82 (red) and W41 (blue) for PLAFP (light gray) in **B** aqueous solution and **C** membrane environment.

three replicas that completed this process within the simulation time (Fig. 8h). In the final inserted state h, the PA head group still interacts with R82, but also with the nearby polar residues T27 and N84. The head group is not completely buried inside PLAFP and is accessible for interactions from the outside. PA unbinding was not observed during the simulations.

During the simulations, we did observe an alternative insertion mechanism in two of the replicas. Here, the lipid does not insert between L_A and L_C, but in the interface between L_C, β_D and α_A (Fig. 8c). The insertion occurred in both cases with one of the tails first resulting in state d, which is similar to state g, but the lipid ester group is not interacting with W115, and the lipid head group sticks out. In one of the two replicas, state d transitioned into state h after 200 ns. Overall, the insertion process is varied, but the eventual bound pose shown in (Fig. 8h) is highly consistent across bound poses.

3.3. *PLAFP-PA complex does not bind to plasma membranes*

To examine if the PLAFP-PA complex is soluble, we simulated its behavior when placed adjacent to membranes, as in Fig. 2B. In the simulations the PLAFP-PA complex is initially positioned directly above the membrane surface, and during half of the 30 simulation replicas, the protein immediately diffuses away and stays in the center of the water phase between the two bilayers of the periodic box (Movie S3). In the other half of the simulation trajectories, PLAFP-PA interacts with the C-terminal α-helix positioning the helix surface in between the membrane surface and the rest of the protein. The quantification of these interactions in Fig. 5 shows that with the insertion of PA all interactions between the membrane surface and the two amino acids W41 and R82 are lost. The interactions between the C-terminal helix and the membrane increase significantly compared to the interaction between the membrane and PLAFP alone, and the interactions are strong enough to keep PLAFP associated to the membrane. In only one of the replica simulations, we observe that PLAFP unbinds within the simulation time after an initial binding with the C-terminal helix. Nevertheless, significantly more replica simulations with PLAFP-PA did not bind to the membrane compared to PLAFP suggesting that PLAFP-PA has a higher dissociation constant. The PLAFP-PA complex would thus be the species most likely to travel large distances through the phloem to an unknown target elsewhere in the plant.

4. Discussion

Our goal was to understand the mechanism of the PLAFP-PA interaction in response to abiotic stress. Previous data had shown that the signaling compound ABA is expressed during drought stress and upregulates *PLAFP* expression as well as PA production (Ali et al., 2020; McLoughlin and Testerink, 2013; Barbaglia et al., 2016). Phospholipids are produced in the ER Schmid (2021) and transported to the plasma membrane. Similarly, PLAFP is associated with PM and ER as well, though it predominantly appears in a spotted pattern along the periphery of the cell (Fig. 3). This pattern could possibly indicate an association with plasmodesmata, given a similar localization pattern in live cells Ishikawa et al. (2017), but other alternatives such as lipid raft association may also be possible. It was suggested that PLAFP binds to PA generated in the plasma membrane by phospholipases, sequesters it away from the aqueous environment and moves it systemically through the phloem stream to its target tissue (Benning et al., 2012; Barbaglia and Hoffmann-Benning, 2016; Barbaglia et al., 2016; Koenig et al., 2020). However, the mechanism and biological possibility of such interactions remained unclear. Our proposed mechanism for the binding, association, and unbinding for PLAFP is outlined in Fig. 9.

In the simulations described here, PLAFP demonstrated a high affinity for and interaction with the phospholipids in the plasma membrane (Figs. 6, 9A). However, this membrane association of PLAFP is not specifically mediated by PA interaction (Fig. 5) Instead we propose that PLAFP may encounter PA by either scooting along the membrane surface until it finds PA, or undergoing multiple association and dissociation events until it binds in close proximity to PA by chance. Since PLAFP did not unbind after penetrating the membrane surface in the simulations, we propose that it is more likely that PLAFP drifts along the membrane surface until the protein encounters PA.

Upon membrane contact, the amino acids W41 and R82 anchor in the membrane, and separate their respective loops to expose a hydrophobic cavity (Figs. 7, 9B). Although we did not explicitly simulate the lipid extraction process, instead using PLAFP in aqueous solution to quantify insertion, we propose that the PA head group interacts with R82, anchoring the lipid near PLAFP, and that the biggest energy barrier for the PA extraction is to get at least one of the tails out of the membrane core. Acyl tail desorption from the membrane may occur by the β_I, β_F-β-sheet surface of PLAFP turning towards the membrane, shielding the hydrophobic acyl tail from solution. The β-sheet surface demonstrated significant interaction in our simulations (Fig. 5). Afterwards, the ester group of one lipid tail might coordinate to W41 allowing the tail to be pulled upwards (Fig. 9C). We expect a much lower energy barrier for the extraction of the second lipid tail after the first lipid tail is outside the membrane surface. Another pathway leading to insertion (Fig. 9D) might occur over states **e-f-g-h**, but further investigations are required in future studies to quantify the relative contributions of alternative binding pathways at the membrane-protein interface.

Based on experimental studies, the hypothesis is that PLAFP transports specifically PA Benning et al. (2012). While lipid ligand specificity

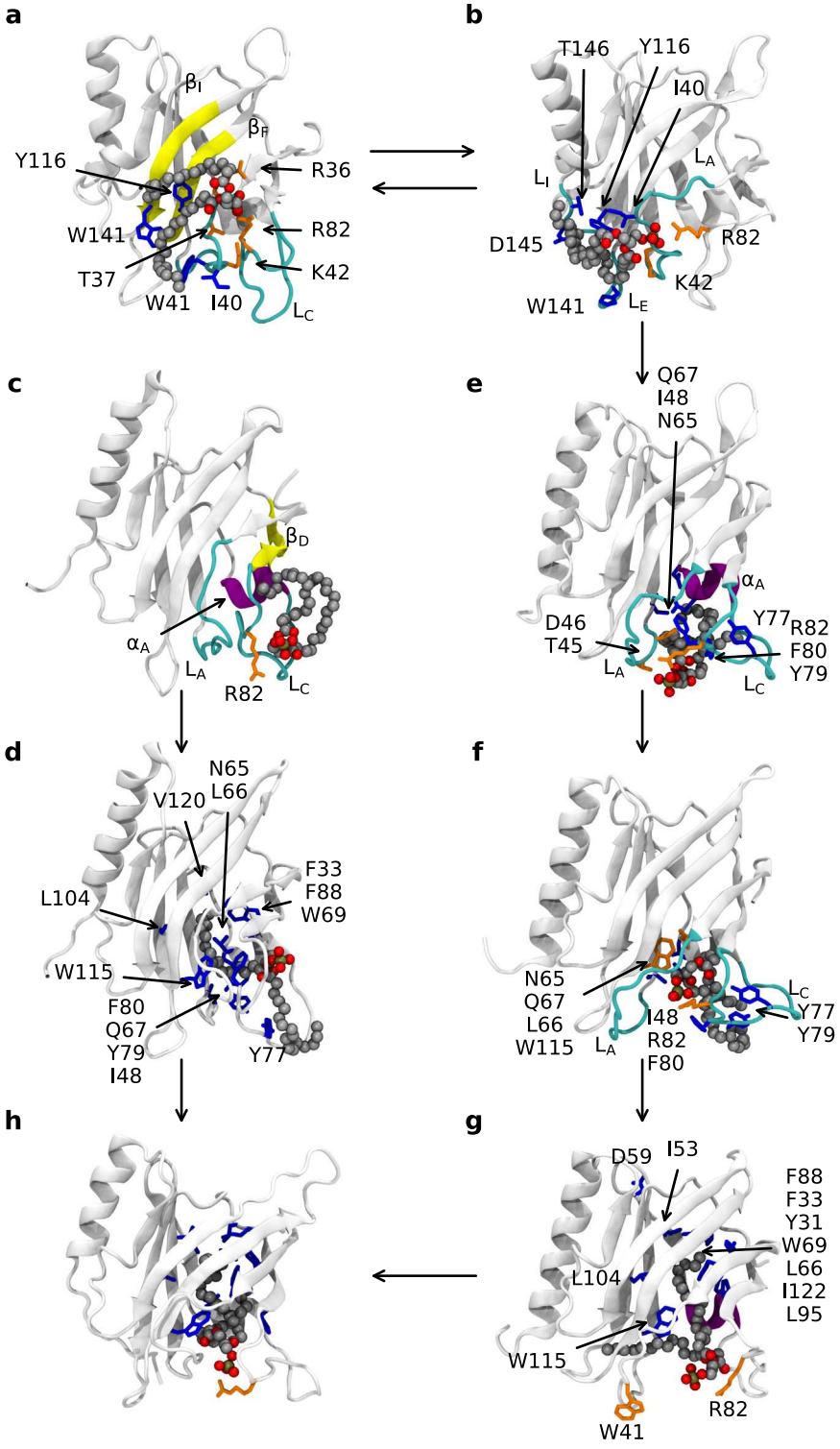

Fig. 8. PA binding traps **a**, **b** and insertion pathways **e-f-g-h**, **c-d-h** into PLAFP. Secondary structure elements referenced in the text are colored according to the type of secondary structure with yellow β-sheet, purple α-helix, and cyan turn. Secondary structure labels correspond to Fig. 2A. Amino acids that have significant contacts to PA are shown in orange if the contact is to the phosphate head group and in blue if it is to the glycerol group or acyl chains.

is beyond the scope of this study, we want to discuss hypotheses for a potential PLAFP selectivity from a thermodynamic and a kinetic perspective based on the results of this study. In a thermodynamic context, PA has the smallest head group, which may mitigate steric hindrance with protein residues identified by our simulations as critical for lipid binding; larger phospholipid headgroups are more likely to clash with amino acids in the binding pocket of PLAFP and thereby destabilize complex formation. Kinetically, the driving force for our proposed main energy barrier, the extraction of one of the lipid tails, is the coulomb interaction between the anionic lipid and the cationic R82. This interaction is not unique to PA, as all negatively charged phospholipids in the plasma membrane (PA, PI, PG and PS) could interact

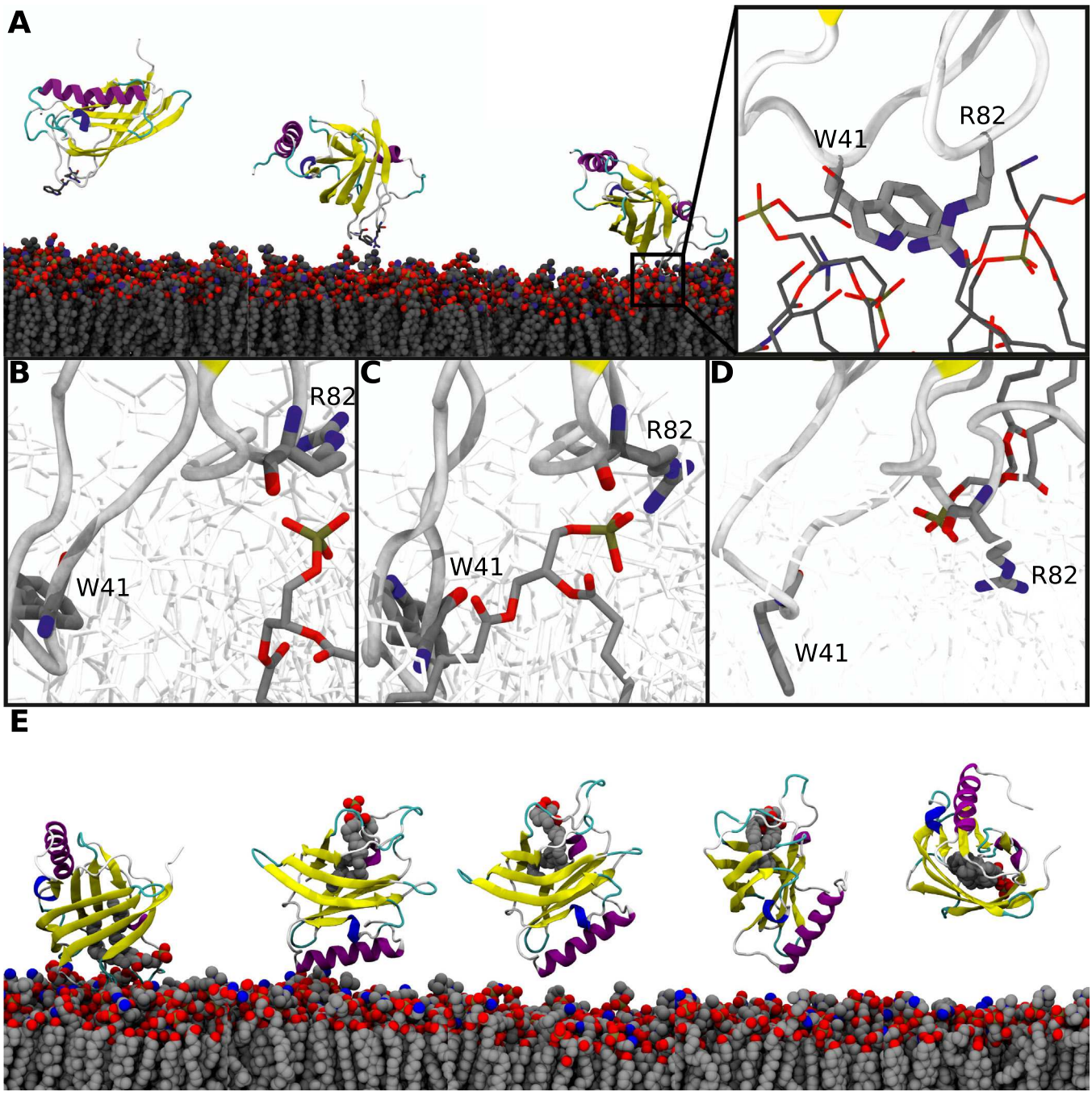

Fig. 9. Hypothesis for PLAFP's PA insertion mechanism from the plasma membrane starting with **A** the membrane association of PLAFP. **B** PA interacts with R82 leading to **C** the lipid tail ester group interacting with W41. **D** PA partially inserted into PLAFP (binding state **e**, cf. Fig. 8). **E** Dissociation from the plasma membrane after PA inserted.

with R82. Larger lipid head groups may weaken the interaction to R82 though, effectively increasing the energy barrier.

After PA is inserted into PLAFP's β-sandwich, the protein dissociates from the plasma membrane (Fig. 9E). This may occur by the protein directly separating from the membrane surface. Alternatively, the membrane interactions with W41 and R82 might be too strong, requiring the protein to fall to the side and slide the C-terminal α-helix between the membrane surface and the rest of the protein (Fig. 9E). This conformational change may facilitate dissociation of the PLAFP-PA complex from the membrane, as the anionic lipid may reduce contacts in the loops, leaving fewer contacts in the C-terminal helix to anchor the complex to the membrane (Fig. 5).

Afterwards, the protein-PA complex moves through the phloem to a currently unknown receptor protein. While it is not yet known whether the protein alone is sufficient to interact with a receptor or if the protein-lipid complex is required to transmit the systemic signal, the protein and lipid together confer an additional layer of specificity for targeted signaling. There is precedent for the participation of lipids during receptor interactions, for example, frizzled-Wnt in mammals Eubelen et al. (2018). Wnt is a developmental regulator that is only active when associated with palmitoleic acid. Crystallography has shown that both, lipid and protein components interact directly with the receptor Janda et al. (2012). Similarly, it is conceivable that in the case of PLAFP-PA, part of the protein and the lipid headgroup need to interact with the

receptor to trigger further signaling. Alternatively, the protein might undergo yet another conformational change with the lipid flipping back out of the hydrophobic pocket at the target site and thus participating in complex-receptor interaction. A third option is that upon arrival at the target tissue, the complex separates and only one component participates in signaling. Examples of protein-lipid complexes involved in signaling have also been show in plants, including phospholipid interactions with transcription factors to regulate gene expression during seedling establishment as well as the transition to flowering (Nakamura et al., 2019; Cai et al., 2020). Further experimentation is needed to resolve the mechanics of PLAFP signaling.

5. Conclusion

Understanding systemic signaling mechanisms in plants is important for genetic applications to increase yield in agricultural crops. In this study, we demonstrated that the phloem-mobile protein PLAFP binds to the plasma membrane and inserts the signaling lipid PA into its β-sandwich. We also provided evidence that the PLAFP-PA complex is less likely to bind to the plasma membrane indicating that the complex might dissociate more easily from the membrane allowing long-distance conductance through the phloem. PLAFP membrane-association is driven by W41 and R82 that anchor the protein into the membrane. PA insertion is initially triggered by interactions to R82, but D46, I48, N65, Q67, A68, Y77, Y79, F80, and W115 do guide the insertion process. In the inserted state, the lipids interact with Y31, F33, I53, I59, I63, L66, W69, F88, L95, L104, W115, V120, and I122 in the hydrophobic pocket. Mutation studies investigating these amino acids can help further elucidate the mechanism of PLAFP action. Future simulation studies should address the PA specificity, receptor proteins for the signal, how PLAFP finds PA in the plasma membrane and the mechanism for PA extraction from the membrane. Ultimately, PLAFP is a potent target protein that could be modulated to allow plant survival in marginal soils and environments, as well as adapt to climatological stresses.

CRediT authorship contribution statement

Martin Kulke: Conceptualization, Methodology, Writing – original draft, Visualization, Supervision, Software. **Evan Kurtz**: Methodology, Investigation, Visualization. **Duncan Boren**: Methodology, Software, Investigation, Visualization. **Dayna M. Olson**: Methodology, Software, Investigation, Visualization. **Amanda M. Koenig**: Conceptualization, Investigation, Visualization, Writing – review & editing. **Susanne Hoffmann-Benning**: Conceptualization, Supervision, Funding acquisition, Writing – review & editing. **Josh V. Vermaas**: Conceptualization, Methodology, Software, Supervision, Funding acquisition, Writing – review & editing.

Declaration of Competing Interest

The authors declare that they have no known competing financial interests or personal relationships that could have appeared to influence the work reported in this paper.

Data availability

Simulation inputs, analysis scripts, and selected outputs are available from Zenodo (https://doi.org/10.5281/zenodo.7847681). Expanded output is available from the authors on request.

Acknowledgments

J.V.V. is supported in part by the U.S. Department of Energy, Office of Basic Energy Sciences under grant number DE-FG02–91ER20021. D. M.O. was supported by the XSEDE Towns et al. (2014) EMPOWER program under National Science Foundation grant number ACI-1548562. This work is supported in part by the National Science Foundation Research Traineeship Program (DGE-1828149) to D.B. This work was supported in part by USDA-NIMSS MICL04147 & 04237 and NSF-EAGER grant number 1841251 to S.H.B. This work was supported in part through computational resources and services provided by the Institute for Cyber-Enabled Research at Michigan State University.

Appendix A. Supporting information

Supplementary data associated with this article can be found in the online version at doi:10.1016/j.plantsci.2023.111900.

References

A. Ali, J.M. Pardo, D.-J. Yun, Desensitization of ABA-signaling: the swing from activation to degradation, Front. Plant Sci. 11 (2020) 379, https://doi.org/10.3389/fpls.2020.00379.

U. Ali, S. Lu, T. Fadlalla, S. Iqbal, H. Yue, B. Yang, Y. Hong, X. Wang, L. Guo, The functions of phospholipases and their hydrolysis products in plant growth, development and stress responses, Prog. Lipid Res. 86 (2022), 101158, https://doi.org/10.1016/j.plipres.2022.101158.

K. Awai, C. Xu, B. Tamot, C. Benning, A phosphatidic acid-binding protein of the chloroplast inner envelope membrane involved in lipid trafficking, Proc. Natl. Acad. Sci. U.S.A. 103 (28) (2006) 10817–10822, https://doi.org/10.1073/pnas.0602754103.

M. Baek, F. DiMaio, I. Anishchenko, J. Dauparas, S. Ovchinnikov, G.R. Lee, J. Wang, Q. Cong, L.N. Kinch, R.D. Schaeffer, C. Millán, H. Park, C. Adams, C.R. Glassman, A. DeGiovanni, J.H. Pereira, A.V. Rodrigues, A.A. van Dijk, A.C. Ebrecht, D. J. Opperman, T. Sagmeister, C. Buhlheller, T. Pavkov-Keller, M.K. Rathinaswamy, U. Dalwadi, C.K. Yip, J.E. Burke, K.C. Garcia, N.V. Grishin, P.D. Adams, R.J. Read, D. Baker, Accurate prediction of protein structures and interactions using a three-track neural network, Sci. (80) 373 (6557) (2021) 871–876, https://doi.org/10.1126/science.abj8754.

J. Bailey-Serres, J.E. Parker, E.A. Ainsworth, G.E.D. Oldroyd, J.I. Schroeder, Genetic strategies for improving crop yields, Nature 575 (7781) (2019) 109–118, https://doi.org/10.1038/s41586-019-1679-0.

A.M. Barbaglia, S. Hoffmann-Benning, Long-distance lipid signaling and its role in plant development and stress response, in: Y. Nakamura, Y. Li-Beisson (Eds.), Lipids in Plant and Algae Development 86, Springer International Publishing, Cham, 2016, pp. 339–361, https://doi.org/10.1007/978-3-319-25979-6_14.

A.M. Barbaglia, B. Tamot, V. Greve, S. Hoffmann-Benning, Phloem proteomics reveals new lipid-binding proteins with a putative role in lipid-mediated signaling, Front. Plant Sci. 7 (2016), https://doi.org/10.3389/fpls.2016.00563.

D. Beglov, B. Roux, Finite representation of an infinite bulk system: solvent boundary potential for computer simulations, J. Chem. Phys. 100 (12) (1994) 9050–9063, https://doi.org/10.1063/1.466711.

U.F. Benning, B. Tamot, B.S. Guelette, S. Hoffmann-Benning, New aspects of phloem-mediated long-distance lipid signaling in plants, Front. Plant Sci. 3 (2012), https://doi.org/10.3389/fpls.2012.00053.

M. Bertoni, F. Kiefer, M. Biasini, L. Bordoli, T. Schwede, Modeling protein quaternary structure of homo- and hetero-oligomers beyond binary interactions by homology, Sci. Rep. 7 (1) (2017) 10480, https://doi.org/10.1038/s41598-017-09654-8.

S. Bienert, A. Waterhouse, T.A. De Beer, G. Tauriello, G. Studer, L. Bordoli, T. Schwede, The SWISS-MODEL Repository-new features and functionality, Nucleic Acids Res 45 (D1) (2017) D313–D319, https://doi.org/10.1093/nar/gkw1132.

G. Cai, S.-C. Kim, J. Li, Y. Zhou, X. Wang, Transcriptional regulation of lipid catabolism during seedling establishment, Mol. Plant 13 (7) (2020) 984–1000, https://doi.org/10.1016/j.molp.2020.04.007.

U. Essmann, L. Perera, M.L. Berkowitz, T. Darden, H. Lee, L.G. Pedersen, A smooth particle mesh Ewald method, J. Chem. Phys. 103 (19) (1995) 8577–8593, https://doi.org/10.1063/1.470117.

M. Eubelen, N. Bostaille, P. Cabochette, A. Gauquier, P. Tebabi, A.C. Dumitru, M. Koehler, P. Gut, D. Alsteens, D.Y.R. Stainier, A. Garcia-Pino, B. Vanhollebeke, A molecular mechanism for Wnt ligand-specific signaling, Science 361 (6403) (2018), eaat1178, https://doi.org/10.1126/science.aat1178.

S.E. Feller, Y. Zhang, R.W. Pastor, B.R. Brooks, Constant pressure molecular dynamics simulation: the Langevin piston method, J. Chem. Phys. 103 (11) (1995) 4613–4621, https://doi.org/10.1063/1.470648.

G.S. Grest, K. Kremer, Molecular dynamics simulation for polymers in the presence of a heat bath, Phys. Rev. A 33 (5) (1986) 3628–3631, https://doi.org/10.1103/PhysRevA.33.3628.

M.S. Grison, L. Brocard, L. Fouillen, W. Nicolas, V. Wewer, P. Dörmann, H. Nacir, Y. Benitez-Alfonso, S. Claverol, V. Germain, Y. Boutté, S. Mongrand, E.M. Bayer, Specific membrane lipid composition is important for plasmodesmata function in arabidopsis, Plant Cell 27 (4) (2015) 1228–1250, https://doi.org/10.1105/tpc.114.135731.

B.S. Guelette, U.F. Benning, S. Hoffmann-Benning, Identification of lipids and lipid-binding proteins in phloem exudates from Arabidopsis thaliana, J. Exp. Bot. 63 (10) (2012) 3603–3616, https://doi.org/10.1093/jxb/ers028.

C.R. Harris, K.J. Millman, S.J. van der Walt, R. Gommers, P. Virtanen, D. Cournapeau, E. Wieser, J. Taylor, S. Berg, N.J. Smith, R. Kern, M. Picus, S. Hoyer, M.H. van Kerkwijk, M. Brett, A. Haldane, J.F. del Río, M. Wiebe, P. Peterson, P. Gérard-

Marchant, K. Sheppard, T. Reddy, W. Weckesser, H. Abbasi, C. Gohlke, T. E. Oliphant, Array programming with NumPy, Nature 585 (7825) (2020) 357–362, https://doi.org/10.1038/s41586-020-2649-2.
J. Huang, S. Rauscher, G. Nawrocki, T. Ran, M. Feig, B.L. De Groot, H. Grubmüller, A. D. MacKerell, CHARMM36m: an improved force field for folded and intrinsically disordered proteins, Nat. Methods 14 (1) (2016) 71–73, https://doi.org/10.1038/nmeth.4067.
W. Humphrey, A. Dalke, K. Schulten, VMD - visual molecular dynamics, J. Mol. Graph. 14 (1) (1996) 33–38, https://doi.org/10.1016/0263-7855(96)00018-5.
J.D. Hunter, Matplotlib: a 2D graphics environment, Comput. Sci. Eng. 9 (3) (2007) 90–95, https://doi.org/10.1109/MCSE.2007.55.
T.K. Hyun, E. van der Graaff, A. Albacete, S.H. Eom, D.K. Großkinsky, H. Böhm, U. Janschek, Y. Rim, W.W. Ali, S.Y. Kim, T. Roitsch, The Arabidopsis PLAT domain protein1 is critically involved in abiotic stress tolerance, PLoS ONE 9 (11) (2014), e112946, https://doi.org/10.1371/journal.pone.0112946.
K. Ishikawa, M. Hashimoto, A. Yusa, H. Koinuma, Y. Kitazawa, O. Netsu, Y. Yamaji, S. Namba, Dual targeting of a virus movement protein to ER and plasma membrane subdomains is essential for plasmodesmata localization, PLoS Pathog. 13 (6) (2017), e1006463, https://doi.org/10.1371/journal.ppat.1006463.
C.Y. Janda, D. Waghray, A.M. Levin, C. Thomas, K.C. Garcia, Structural basis of Wnt recognition by frizzled, Science 337 (6090) (2012) 59–64, https://doi.org/10.1126/science.1222879.
S. Jo, T. Kim, V.G. Iyer, W. Im, CHARMM-GUI: a web-based graphical user interface for CHARMM, J. Comput. Chem. 29 (11) (2008) 1859–1865, https://doi.org/10.1002/jcc.20945.
W.L. Jorgensen, J. Chandrasekhar, J.D. Madura, R.W. Impey, M.L. Klein, Comparison of simple potential functions for simulating liquid water, J. Chem. Phys. 79 (2) (1983) 926–935, https://doi.org/10.1063/1.445869.
M. Källberg, H. Wang, S. Wang, J. Peng, Z. Wang, H. Lu, J. Xu, Template-based protein structure modeling using the RaptorX web server, Nat. Protoc. 7 (8) (2012) 1511–1522, https://doi.org/10.1038/nprot.2012.085.
S.-C. Kim, X. Wang, Phosphatidic acid: an emerging versatile class of cellular mediators, Essays Biochem. 64 (3) (2020) 533–546, https://doi.org/10.1042/EBC20190089.
J.B. Klauda, R.M. Venable, J.A. Freites, J.W. O'Connor, D.J. Tobias, C. Mondragon-Ramirez, I. Vorobyov, A.D. MacKerell, R.W. Pastor, Update of the CHARMM all-atom additive force field for lipids: validation on six lipid types, J. Phys. Chem. B 114 (23) (2010) 7830–7843, https://doi.org/10.1021/jp101759q.
A.M. Koenig, C. Benning, S. Hoffmann-Benning, Lipid trafficking and signaling in plants, in: Lipid Signaling and Metabolism, Elsevier, 2020, pp. 23–44, https://doi.org/10.1016/B978-0-12-819404-1.00002-6.
M. Kulke, S.M. Weraduwage, T.D. Sharkey, J.V. Vermaas, Nanoscale simulation of the thylakoid membrane response to extreme temperatures, Plant Cell Environ. (2023) pce.14609, https://doi.org/10.1111/pce.14609.
J. Lee, X. Cheng, J.M. Swails, M.S. Yeom, P.K. Eastman, J.A. Lemkul, S. Wei, J. Buckner, J.C. Jeong, Y. Qi, S. Jo, V.S. Pande, D.A. Case, C.L. Brooks, A.D. MacKerell, J. B. Klauda, W. Im, CHARMM-GUI input generator for NAMD, GROMACS, AMBER, OpenMM, and CHARMM/OpenMM simulations using the CHARMM36 additive force field, J. Chem. Theory Comput. 12 (1) (2016) 405–413, https://doi.org/10.1021/acs.jctc.5b00935.
L. Li, H. Xie, L. Liang, Y. Gao, D. Zhang, L. Fang, S.O. Lee, J. Luo, X. Chen, X. Wang, L. S. Chang, S. Yeh, Y. Wang, D. He, C. Chang, Increased PrLZ-mediated androgen receptor transactivation promotes prostate cancer growth at castration-resistant stage, Carcinogenesis 34 (2) (2013) 257–267, https://doi.org/10.1093/carcin/bgs337.
C.-C. Lin, Y.-T. Chao, W.-C. Chen, H.-Y. Ho, M.-Y. Chou, Y.-R. Li, Y.-L. Wu, H.-A. Yang, H. Hsieh, C.-S. Lin, F.-H. Wu, S.-J. Chou, H.-C. Jen, Y.-H. Huang, D. Irene, W.-J. Wu, J.-L. Wu, D.J. Gibbs, M.-C. Ho, M.-C. Shih, Regulatory cascade involving transcriptional and N-end rule pathways in rice under submergence, Proc. Natl. Acad. Sci. U.S.A.116 (8) (2019)3300–3309.10.1073/pnas.1818507116.
Q. Liu, Y. Ding, Y. Shi, L. Ma, Y. Wang, C. Song, K.A. Wilkins, J.M. Davies, H. Knight, M. R. Knight, Z. Gong, Y. Guo, S. Yang, The calcium transporter ANNEXIN1 mediates cold-induced calcium signaling and freezing tolerance in plants, EMBO J. 40 (2) (2021), https://doi.org/10.15252/embj.2020104559.
W.J. Lucas, A. Groover, R. Lichtenberger, K. Furuta, S.-R. Yadav, Y. Helariutta, X.-Q. He, H. Fukuda, J. Kang, S.M. Brady, J.W. Patrick, J. Sperry, A. Yoshida, A.-F. López-Millán, M.A. Grusak, P. Kachroo, The plant vascular system: evolution, development and functions, J. Integr. Plant Biol. 55 (4) (2013) 294–388, https://doi.org/10.1111/jipb.12041.
F. McLoughlin, C. Testerink, Phosphatidic acid, a versatile water-stress signal in roots, Front. Plant Sci. 4 (2013), https://doi.org/10.3389/fpls.2013.00525.
R. Mega, F. Abe, J.-S. Kim, Y. Tsuboi, K. Tanaka, H. Kobayashi, Y. Sakata, K. Hanada, H. Tsujimoto, J. Kikuchi, S.R. Cutler, M. Okamoto, Tuning water-use efficiency and drought tolerance in wheat using abscisic acid receptors, Nat. Plants 5 (2) (2019) 153–159, https://doi.org/10.1038/s41477-019-0361-8.
S. Miyamoto, P.A. Kollman, Settle: An analytical version of the SHAKE and RATTLE algorithm for rigid water models, J. Comput. Chem 13 (8) (1992) 952–962, https://doi.org/10.1002/jcc.540130805.
T. Munnik, Phosphatidic acid: An emerging plant lipid second messenger, Trends Plant Sci. 6 (5) (2001) 227–233, https://doi.org/10.1016/S1360-1385(01)01918-5.
R. Munns, R.A. James, B. Xu, A. Athman, S.J. Conn, C. Jordans, C.S. Byrt, R.A. Hare, S. D. Tyerman, M. Tester, D. Plett, M. Gilliham, Wheat grain yield on saline soils is improved by an ancestral Na. transporter gene, Nat. Biotechnol. 30 (4) (2012) 360–364, https://doi.org/10.1038/nbt.2120.
A. Mustroph, M.E. Zanetti, C.J.H. Jang, H.E. Holtan, P.P. Repetti, D.W. Galbraith, T. Girke, J. Bailey-Serres, Profiling translatomes of discrete cell populations resolves altered cellular priorities during hypoxia in Arabidopsis, Proc. Natl. Acad. Sci. U.S.A. 106 (44) (2009) 18843–18848, https://doi.org/10.1073/pnas.0906131106.
Y. Nakamura, Y.-C. Lin, S. Watanabe, Y.-c. Liu, K. Katsuyama, K. Kanehara, K. Inaba, High-resolution crystal structure of Arabidopsis FLOWERING LOCUS T illuminates its phospholipid-binding site in flowering, iScience 21 (2019) 577–586, https://doi.org/10.1016/j.isci.2019.10.045.
B.K. Nelson, X. Cai, A. Nebenführ, A multicolored set of in vivo organelle markers for co-localization studies in Arabidopsis and other plants: fluorescent organelle markers, Plant J. 51 (6) (2007) 1126–1136, https://doi.org/10.1111/j.1365-313X.2007.03212.x.
M. Notaguchi, S. Okamoto, Dynamics of long-distance signaling via plant vascular tissues Front. Plant Sci. 2015.10.3389/fpls.2015.00161.
S. Ovchinnikov, H. Park, N. Varghese, P.S. Huang, G.A. Pavlopoulos, D.E. Kim, H. Kamisetty, N.C. Kyrpides, D. Baker, Protein structure determination using metagenome sequence data, Sci. (80) 355 (6322) (2017) 294–298, https://doi.org/10.1126/science.aah4043.
J.C. Phillips, D.J. Hardy, J.D. Maia, J.E. Stone, J.V. Ribeiro, R.C. Bernardi, R. Buch, G. Fiorin, J. Hénin, W. Jiang, R. McGreevy, M.C. Melo, B.K. Radak, R.D. Skeel, A. Singharoy, Y. Wang, B. Roux, A. Aksimentiev, Z. Luthey-Schulten, L.V. Kalé, K. Schulten, C. Chipot, E. Tajkhorshid, Scalable molecular dynamics on CPU and GPU architectures with NAMD, J. Chem. Phys. 153 (4) (2020) 44130, https://doi.org/10.1063/5.0014475.
D.K. Ray, N.D. Mueller, P.C. West, J.A. Foley, Yield trends are insufficient to double global crop production by 2050, PLoS ONE 8 (6) (2013), e66428, https://doi.org/10.1371/journal.pone.0066428.
M. Renatus, R.A. Engh, M.T. Stubbs, R. Huber, S. Fischer, U. Kohnert, W. Bode, Lysine 156 promotes the anomalous proenzyme activity of tPA: X-ray crystal structure of single-chain human tPA, EMBO J. 16 (16) (1997) 4797–4805, https://doi.org/10.1093/emboj/16.16.4797.
A. Rice, J. Wereszczynski, Probing the disparate effects of arginine and lysine residues on antimicrobial peptide/bilayer association, Biochim. Biophys. Acta - Biomembr. 1859 (10) (2017) 1941–1950, https://doi.org/10.1016/j.bbamem.2017.06.002.
A. Roy, A. Kucukural, Y. Zhang, I-TASSER: a unified platform for automated protein structure and function prediction, Nat. Protoc. 5 (4) (2010) 725–738, https://doi.org/10.1038/nprot.2010.5.
A.P. Ruymgaart, R. Elber, Revisiting molecular dynamics on a CPU/GPU system: water kernel and SHAKE parallelization, J. Chem. Theory Comput. 8 (11) (2012) 4624–4636, https://doi.org/10.1021/ct300324k.
F.B. Sheinerman, C.L. Brooks, Calculations on folding of segment B1 of streptococcal protein G, J. Mol. Bio. 278 (2) (1998) 439–456, https://doi.org/10.1006/jmbi.1998.1688.
J. Söding, Protein homology detection by HMM-HMM comparison, Bioinformatics 21 (7) (2005) 951–960, https://doi.org/10.1093/bioinformatics/bti125.
K.M. Schmid, Lipid metabolism in plants, in: Biochemistry of Lipids, Lipoproteins and Membranes, Elsevier, 2021, pp. 121–159, https://doi.org/10.1016/B978-0-12-824048-9.00011-0.
Y. Song, F. DiMaio, R.Y.R. Wang, D. Kim, C. Miles, T.J. Brunette, J. Thompson, D. Baker, High-resolution comparative modeling with RosettaCM, Structure 21 (10) (2013) 1735–1742, https://doi.org/10.1016/j.str.2013.08.005.
G. Studer, C. Rempfer, A.M. Waterhouse, R. Gumienny, J. Haas, T. Schwede, QMEANDisCo—distance constraints applied on model quality estimation, Bioinformatics 36 (6) (2020) 1765–1771, https://doi.org/10.1093/bioinformatics/btz828.
F. Takahashi, K. Shinozaki, Long-distance signaling in plant stress response, Curr. Opin. Plant Biol. 47 (2019) 106–111, https://doi.org/10.1016/j.pbi.2018.10.006.
C. Testerink, T. Munnik, Phosphatidic acid: a multifunctional stress signaling lipid in plants, Trends Plant Sci. 10 (8) (2005) 368–375, https://doi.org/10.1016/j.tplants.2005.06.002.
C. Testerink, T. Munnik, Molecular, cellular, and physiological responses to phosphatidic acid formation in plants, J. Exp. Bot. 62 (7) (2011) 2349–2361, https://doi.org/10.1093/jxb/err079.
C. Testerink, P.B. Larsen, D. van der Does, J.A. van Himbergen, T. Munnik, Phosphatidic acid binds to and inhibits the activity of Arabidopsis CTR1, J. Exp. Bot. 58 (14) (2007) 3905–3914, https://doi.org/10.1093/jxb/erm243.
The UniProt Consortium, UniProt: a hub for protein information, Nucleic Acids Res. 43 (D1) (2015) D204–12, https://doi.org/10.1093/nar/gku989.
J. Towns, T. Cockerill, M. Dahan, I. Foster, K. Gaither, A. Grimshaw, V. Hazlewood, S. Lathrop, D. Lifka, G.D. Peterson, R. Roskies, J.R. Scott, N. Wilkins-Diehr, XSEDE: accelerating scientific discovery, Comput. Sci. Eng. 16 (5) (2014) 62–74, https://doi.org/10.1109/MCSE.2014.80.
M. Uemura, R.A. Joseph, P.L. Steponkus, Cold acclimation of Arabidopsis thaliana: effect on plasma membrane lipid composition and freeze-induced lesions, Plant Physiol. 109 (1) (1995) 15–30, https://doi.org/10.1104/pp.109.1.15.
G. Van Rossum, F.L. Drake, Python 3 Reference Manual, CreateSpace, Scotts Valley, CA, 2009.
X. Wang, K.D. Chapman, Lipid signaling in plants, Front. Plant Sci. 4 (2013), https://doi.org/10.3389/fpls.2013.00216.
X. Wang, W. Zhang, W. Li, G. Mishra, Phospholipid signaling in plant response to drought and salt stress, in: M.A. Jenks, P.M. Hasegawa, S.M. Jain (Eds.), Advances in Molecular Breeding Toward Drought and Salt Tolerant Crops, Springer, Netherlands, Dordrecht, 2007, https://doi.org/10.1007/978-1-4020-5578-2.
Z. Wang, N.S. Anderson, C. Benning, The phosphatidic acid binding site of the arabidopsis trigalactosyldiacylglycerol 4 (TGD4) protein required for lipid import into chloroplasts, J. Biol. Chem. 288 (7) (2013) 4763–4771, https://doi.org/10.1074/jbc.M112.438986.

E. Wang, P. Martre, Z. Zhao, F. Ewert, A. Maiorano, R.P. Rötter, B.A. Kimball, M. J. Ottman, G.W. Wall, J.W. White, M.P. Reynolds, P.D. Alderman, P.K. Aggarwal, J. Anothai, B. Basso, C. Biernath, D. Cammarano, A.J. Challinor, G. De Sanctis, J. Doltra, B. Dumont, E. Fereres, M. Garcia-Vila, S. Gayler, G. Hoogenboom, L. A. Hunt, R.C. Izaurralde, M. Jabloun, C.D. Jones, K.C. Kersebaum, A.-K. Koehler, L. Liu, C. Müller, S.N. Kumar, C. Nendel, G. O'Leary, J.E. Olesen, T. Palosuo, E. Priesack, E. EyshiRezaei, D. Ripoche, A.C. Ruane, M.A. Semenov, I. Shcherbak, C. Stöckle, P. Stratonovitch, T. Streck, I. Supit, F. Tao, P. Thorburn, K. Waha, D. Wallach, Z. Wang, J. Wolf, Y. Martre, S. Asseng, The uncertainty of crop yield projections is reduced by improved temperature response functions, Nat. Plants 3 (8) (2017) 17102, https://doi.org/10.1038/nplants.2017.102.

J.V. Vermaas, E. Tajkhorshid, Differential Membrane Binding Mechanics of Synaptotagmin Isoforms Observed in Atomic Detail, Biochemistry 56 (1) (2017) 281–293, https://doi.org/10.1021/acs.biochem.6b00468.

X. Wang, Lipid signaling, Curr. Opin. Plant Biol. 7 (3) (2004) 329–336, https://doi.org/10.1016/j.pbi.2004.03.012.

A. Waterhouse, M. Bertoni, S. Bienert, G. Studer, G. Tauriello, R. Gumienny, F.T. Heer, T. A. De Beer, C. Rempfer, L. Bordoli, R. Lepore, T. Schwede, SWISS-MODEL: Homology modelling of protein structures and complexes, Nucleic Acids Res. 46 (W1) (2018) W296–W303, https://doi.org/10.1093/nar/gky427.

E.L. Wu, X. Cheng, S. Jo, H. Rui, K.C. Song, E.M. Dávila-Contreras, Y. Qi, J. Lee, V. Monje-Galvan, R.M. Venable, J.B. Klauda, W. Im, CHARMM-GUI membrane builder toward realistic biological membrane simulations, J. Comput. Chem. 35 (27) (2014) 1997–2004, https://doi.org/10.1002/jcc.23702.

Y. Yang, E. Faraggi, H. Zhao, Y. Zhou, Improving protein fold recognition and template-based modeling by employing probabilistic-based matching between predicted one-dimensional structural properties of query and corresponding native properties of templates, Bioinformatics 27 (15) (2011) 2076–2082, https://doi.org/10.1093/bioinformatics/btr350.

J. Yang, R. Yan, A. Roy, D. Xu, J. Poisson, Y. Zhang, The I-TASSER suite: Protein structure and function prediction (2014). 10.1038/nmeth.3213.

J. Yang, I. Anishchenko, H. Park, Z. Peng, S. Ovchinnikov, D. Baker, Improved protein structure prediction using predicted interresidue orientations, Proc. Natl. Acad. Sci. U. S. A 117 (3) (2020) 1496–1503, https://doi.org/10.1073/pnas.1914677117.

H. Zhang, J. Zhu, Z. Gong, J.-K. Zhu, Abiotic stress responses in plants, Nat. Rev. Genet 23 (2) (2022) 104–119, https://doi.org/10.1038/s41576-021-00413-0.

Y. Zhang, I-TASSER server for protein 3D structure prediction, BMC Bioinforma. 9 (1) (2008) 40, https://doi.org/10.1186/1471-2105-9-40.